

# PW-Self: Patch-Wise Self-Supervised Visual Representation Learning

Ali Javidani<sup>1\*</sup>, Mohammad Amin Sadeghi<sup>1,2</sup>, Babak Nadjar Araabi<sup>1</sup>

<sup>1</sup> School of Electrical and Computer Engineering, College of Engineering, University of Tehran, Tehran, Iran

<sup>2</sup> Qatar Computing Research Institute, Doha, Qatar

\*alijavidani@ut.ac.ir

**Abstract-** Self-supervised visual representation learning traditionally focuses on image-level instance discrimination. Our study introduces an innovative dimension by integrating patch-level discrimination into these methodologies. This integration allows for the simultaneous analysis of both local and global visual features, thereby enriching the quality of the representations learned. Initially, the original images undergo spatial augmentation. Subsequently, we employ a distinctive photometric patch-level augmentation, where each patch is individually augmented, independent from other patches within the same view. This approach generates a diverse training dataset with distinct color variations in each segment. The augmented images are then processed through a self-distillation learning framework, utilizing the Vision Transformer (ViT) as its backbone. The proposed method minimizes the representation distances across both image and patch levels to capture details from macro to micro perspectives. To this end, we present a simple yet effective patch-matching algorithm that can find the corresponding patches across the augmented views. Thanks to the efficient structure of the patch-matching algorithm, our method reduces computational complexity compared to similar approaches. Consequently, we achieve an advanced understanding of the model without adding significant computational requirements. We have extensively pre-trained our method on datasets of varied scales, such as Cifar10, ImageNet-100, and ImageNet-1K. It demonstrates superior performance over state-of-the-art self-supervised representation learning methods in image classification and downstream tasks, such as copy detection and image retrieval. The implementation of our method is accessible on [GitHub](#).

**Keywords-** Self-Supervised Learning; Patch-Wise Representation Learning; Self-Distillation; Patch-level Augmentation; Patch-Matching;

## 1. Introduction

Self-supervised representation learning growth was coupled with the appearance of instance discrimination. Instance discrimination has gained considerable attention during the last few years [1-10]. It behaves the samples in a mini-batch as separate classes. As a result, their representations are pushed away from each other. SimCLR [9] and MoCo [8] are among the two famous frameworks that could benefit from it. However, instance discrimination has its downsides. Firstly, the assumption of different classes for every sample in the mini-batch is not necessarily correct. This is because two or more samples in a mini-batch can imply the same concept and thus have the same labels. Secondly, pushing away the representations for every sample requires  $O(n^2)$  time complexity which hardens the training process. Thirdly, low-level features which contribute mostly to the details of an image are not captured.

Many works in the literature address the first and second problems. Clustering-based methods aim to tackle the first problem [11-15]. SwAV [14], PCL [13], and oBoW [11] by integrating online clustering as one of the steps in representation learning, could surge the performance of contrastive methods. Non-contrastive methods focus on avoiding degenerating solutions without pushing away the representations of every sample in the batch [16-24]. Their training speed has been boosted in comparison with contrastive methods. BYOL [23], SimSiam [20], and DINO [21] are examples of methods in this category. However, little research has been conducted to address the third problem [25, 26]. Most of the existing papers usually work on image-level features. Considering image-level features has led the machine to comprehend the overall concept of the image. However, some details that can play a significant role in determining the label of the image, may be disregarded. As a result, this area still seems to be open.

The main focus of our approach in this paper is to take a step towards a better understanding of the details of images when training in the self-supervised learning fashion. This is done by regulating the consistency loss for not only the augmented images but also the local regions, e.g., patches, inside the augmented variants. The latter results in generating additional loss terms which can guide the model to understand the details of images more prominently. Our main contributions to this work are as follows:

- Patch-level augmentation: To the best of our knowledge, the idea of individually augmenting patches, independent from each other and the whole image, is an innovative approach that has not been explored previously. It can redefine the boundaries of feature extraction and representation in deep learning algorithms, especially in the context of vision transformers.
- Patch-matching algorithm: a simple yet effective patch-matching algorithm that finds the corresponding patches across the augmented views in  $O(1)$ . It can be highly useful in self-supervised representation learning frameworks.

- PW-Self: a patch-wise self-supervised visual representation learning model that uniquely integrates local and global loss calculations into several cohesive dual loss functions, enabling a more comprehensive understanding of visual data at both micro and macro levels.
- Compare the proposed PW-Self method with other approaches, achieving state-of-the-art results on small, medium, and large-scale datasets

PW-Self is different from the literature on patch-wise self-supervised representation learning [25-27]. In SelfPatch the invariance constraint is enforced against each patch and its neighbors [25]. However, in some cases, adjacent patches may not share the same concept. In addition, it cannot help the machine to distinguish between different parts of an object. In contrast, our method, by pulling the same object parts' representations across the augmented images, guides the model to learn them effectively. In EsViT a multi-stage architecture with sparse self-attention is proposed [26]. Then, for capturing fine-grained features, a region-matching pretraining task is done. This task is done by finding the patch with the highest cosine similarity score for each patch. This approach has two main drawbacks. First, there is no guarantee that the most relevant patch is discovered by calculating the cosine similarity, especially at the early stages of pretraining where the network has not become enough mature. Second, this process requires  $O(T^2)$  time complexity (where  $T$  is the number of patches) to find relevant patches. Thanks to the proposed patch-matching algorithm, our method does not suffer from either of the mentioned limitations. It finds the most relevant patch in  $O(1)$ . In [27], the assumption is to push away the representations of two local views of the same image as they might contain dissimilar content. However, this assumption may not always be true. In contrast, the proposed PW-Self method identifies corresponding local regions across augmented views and minimizes the distance between their representations.

The rest of the paper is organized as follows. In section 2, the works related to our approach are reviewed. Section 3 explains the proposed PW-Self method and the theory behind that extensively. In section 4, the results of PW-Self and a comparison with the state-of-the-art methods on various datasets are reported. In section 5, discussions on the computational complexities, and effects of the parameters related to our method are debated.

## 2. Related Works: Self-Supervised Representation Learning

### 2.1 Contrastive Methods

SimCLR stands out as the first and one of the most successful approaches that is based on contrastive loss [9]. It operates by extracting two distinct augmentations of each image within a mini-batch and subsequently performs instance classification, aiming to make the representations of augmented images from the same source image close while keeping representations from different images apart. SimCLR was extended to SimCLR-v2 [28], which employed massive task-agnostic unlabeled data for pre-training network weights and fine-tuning with labeled data. The model's scalability and performance depend on the mini-batch size that presents memory challenges. MoCo introduced a solution with separate query and key branches, allowing gradients from contrastive loss to backpropagate only through the query branch [8]. MoCo-v2 achieved even better results by using multiple queries [29], and Moco-v3 improved stability using ViT as a backbone [30]. Another method, Contrastive Predictive Coding (CPC), aimed to detect anomalies while learning self-supervised representations by predicting future data in latent space with probabilistic contrastive loss, emphasizing the capture of highly informative content for prediction [10]. Furthermore, Self-Distilled Self-Supervised Learning (SDSSL) was developed in which intermediate representations learn from the representation of the ultimate layer of the network through a self-distillation process [31].

Some works focused on boosting contrastive learning performance by selecting harder negative samples. In [7], the authors proposed hard negative mixing strategies at the feature level to generate synthetic samples. In [32], the mutual information between views is reduced to learn effective views. In a similar work, the ContrastiveCrop framework is proposed in which object localization is applied to craft better contrastive views [33]. Authors in NNCLR [4] claim that by finding the nearest samples to the anchor and treating them as positives, they could enhance the performance of contrastive learning. In [1, 2], different strategies for selecting difficult negative samples are proposed. Another work addresses this issue by generating hard negative examples [34]. Recent work identifies false negatives in the mini-batch and proposes cancellation and attraction strategies towards them to utilize their related information effectively [35]. In TMCT, a third network with momentum is used to provide the targets for the final model learning [36]. Self-supervised contrastive learning has also been successful in various domains, including time series analysis [37], and stock prediction [38].

### 2.2 Clustering-based Methods

Instance discrimination has demonstrated favorable performance enhancements within the domain of self-supervised representation learning. However, this methodology treats images from the same class as distinct instances, resulting in the divergence of their embeddings. In practical terms, when two images of the same class coexist within the same mini-batch, the applied loss function compels their representations, which is undesirable. To mitigate the contrastive learning limitation, some studies have integrated clustering into the overall framework [11-15]. As a first attempt, in Deep Embedded Clustering (DEC) a general framework was proposed in which an autoencoder is trained and, at the same time, the representations in the latent space are clustered [39]. Caron *et al.* trained a Convolutional Neural Network to extract features from the input and by performing clustering, they provided pseudo-labels for the network to be trained properly [15].

More recent research has combined contrastive learning and clustering to achieve superior results. In one instance, authors in [14], explored clustering with the Sinkhorn-Knopp transform after feature extraction from augmented images, specifying a predetermined number of clusters and assigning image representations to prototypes. Another approach, Prototypical Contrastive Learning (PCL), introduced prototypes as centroids for clusters of similar images, with each image assigned to multiple prototypes of varying granularity [13]. The training aimed to bring image embeddings closer to associated prototypes by minimizing a ProtoNCE loss function. In a similar work, the OBoW method aimed to predict visual words constructed from original images using augmented versions, utilizing a teacher-student network structure where the teacher branch provided visual words and the student branch learned representations with momentum-based updates [11]. In the MCVT framework, cluster-based and info-based contrastive losses were combined to capture high-level and low-level features respectively [40]. In addition, the authors in [41] proposed Self-Supervised Pyramid Representation Learning (SS-PRL) to generate pyramid representations at the patch level by training appropriate prototypes. This framework also incorporates supplementary learners to analyze and establish connections between the inherent semantic information present within an image.

### 2.3 Non-Contrastive Methods

In contrast to contrastive learning, which considers both negative and positive pairs, in non-contrastive learning, the focus is solely on positive samples. An example of a non-contrastive approach is BYOL (Bootstrap Your Own Latent) [23]. BYOL extracts two sets of views from an image and passes them through encoders, with the target encoder being an exponential moving average of the online encoder. The loss is computed as the mean squared error between the online and target encoders. An extension of BYOL, MYOW, takes a different approach by using two nearby distinct samples instead of two different augmentations of the same image [22]. This results in significant performance improvements over BYOL. DINO utilizes self-distillation and involves both a teacher and student network adopting the Vision Transformer (ViT) architecture [21]. Notably, the teacher network employs momentum, maintaining exponentially weighted average weights of the student network. Additional centering and sharpening modules are used to prevent trivial solutions. Following BYOL's success, the authors in MSBReg, by combining three loss terms capturing information from multiple sources, could further increase the performance [42]. Furthermore, SimSiam demonstrates remarkable performance even without auxiliary structures like negative samples, clustering, or moving averages [20]. This makes it computationally efficient and results in outperforming other self-supervised networks, such as SimCLR and BYOL, particularly in terms of training with smaller batch sizes.

A recent category in non-contrastive approaches aims to maximize the information content within representation vectors while preventing the issue of representation collapse, as discussed in prior studies [43]. These methods introduce specific constraints into their objective functions to deter the representations from converging into a constant vector. In one instance, this is achieved by performing whitening on the latent space obtained from processing diverse augmentations of the same image [19]. In another approach, the empirical cross-correlation matrix is computed and optimized to resemble the identity matrix, a framework known as Barlow Twins, to reduce redundancy among inputs [18]. Complementing this work, the authors in [16] introduced an additional loss term that elevates the variance among images within the mini-batch above a predefined threshold, yielding more robust outcomes. Feng *et al.* proposed a data augmentation method to address the problem of insufficient training data [44]. In this work, an encoder-decoder was trained in which by disentangling the features, they could solve the person reidentification task. Further exploration by Zhang *et al.* involved randomly grouping feature dimensions and comparing them with basis norms [45]. Wang *et al.* proposed TWIST, which enforces similarity in the class distributions of two augmented images by introducing a constraint on mutual information maximization in the cost function to prevent collapse [46]. Another work, with the aid of self-supervised learning, investigated the issue of unfairness in recommendation systems by introducing a fairness-based hierarchical mutual information maximization component [47]. Additionally in Self-Classifier, modifications to the standard cross-entropy characterized by a uniform prior assumption on predicted labels led to enhanced results [48].

## 3. Proposed Patch-Wise Self-Supervised Representation Learning

### 3.1 An Explanation of DINO and Its Limitation

The recent self-supervised framework DINO, with the aid of knowledge distillation, could utilize the power of Vision Transformers (ViTs) for the self-supervised representation learning problem [21]. In this framework, by performing various kinds of augmentations, the global and local crops of an original image are extracted. The global crops pass through the teacher and both the global and local crops pass through the student network. The idea is to pull representations resulting from the outputs of these two networks. As a result, the CLS embedding, which is the representation of the whole image, is extracted for each augmented image. Then, the cross-entropy loss between the outputs of student and teacher networks is computed to match the representation of the local image with the representation of the global variant.

In this framework, the emphasis is placed solely on the CLS tokens, serving as representatives of the entire input image, while tokens associated with image patches are disregarded. Essentially, the model captures image-level representations while neglecting patch-level representations. While it is shown that the image-level representation constraint leads the model to learn a meaningful representation, this constraint may not be sufficient for acquiring an exhaustive representation space. For instance, when an image encompasses multiple objects, matching representations of the entire image across augmented views may lead to confusion regarding the primary focus of the image. However, introducing specific constraints, such as ensuring consistency in representations of local regions, could enhance the

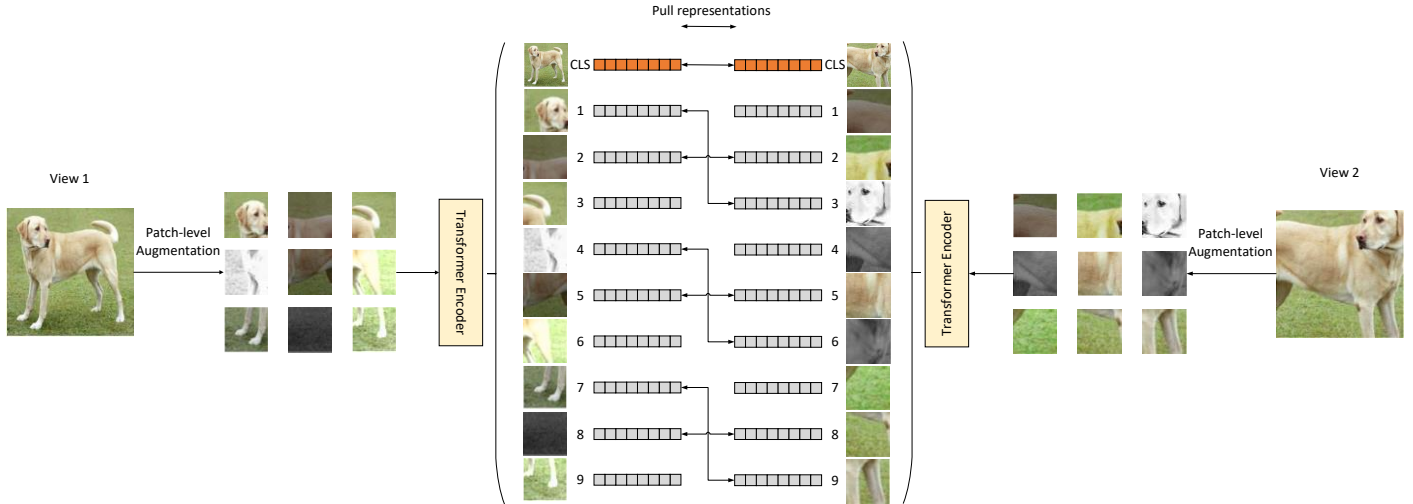


Figure 1 An image of a dog is spatially augmented via random crop and flip operations in two ways to obtain view1 and view2. Then, the two views undergo patch-level augmentation in which each patch is independently augmented using photometric augmentations. Subsequently, they are fed to the Vision Transformer (ViT) encoders. The ViT encoder extract representations for both the entire image (CLS tokens) and each patch. PW-Self minimizes the representation distance between CLS tokens as well as corresponding patches across views, leveraging the proposed patch-matching algorithm. Pulling the CLS tokens gives the model an idea of the entire object in the image; while minimizing the distance between the patch tokens guides the model towards a better understanding of the details within the image.

model’s understanding of image components. This approach facilitates a discernible differentiation between object representations. Even if the image contains only a single object, by imposing additional specific restrictions, the model is anticipated to develop an enhanced understanding of the various components of the object. For example, if the image depicts a dog, by pulling representations of the dog’s head in the augmented images, the model can distinguish between the head and other parts of the dog more effectively.

### 3.2 Proposed Idea: Local-Global Matching

Our key idea is to capture local information inside the image patches and use it alongside the global information to train the model more effectively. One approach to acquiring local information is to match correspondent patches across augmented images which leads to generating additional loss terms. We think these supplemental loss terms can serve as valuable inductive biases for the model facilitating the capture of abstraction levels with finer granularities. This is in contrast to the DINO, where such loss terms were entirely disregarded. Consequently, our approach empowers the model not only to comprehend the overarching concepts within an image but also to develop a profound understanding of its constituent details.

Figure 1 illustrates the overall idea of PW-Self using ViT encoders. The proposed PW-Self framework is as follows: The original image is augmented into two views using spatial augmentations. Spatial augmentations are the ones that affect the positions of pixels such as crop, resize, and horizontal flip. The two augmented views are then divided into patches, and each patch undergoes patch-level augmentations in which each patch is augmented independently of others (3.3). The resulting images are fed to the ViT encoder network. The encoder network yields CLS tokens and tokens related to the patches inside the images. The correspondent patches across augmented views are found with the aid of the patch-matching algorithm (3.4). Finally, the loss is calculated by matching both the CLS tokens and the correspondent patches (3.5).

Our framework incorporates a dual-network architecture consisting of a student network and a teacher network, an approach inspired by the principles of self-distillation [21]. It facilitates effective learning and knowledge transfer within the self-supervised learning paradigm without the need for negative samples. For feeding the images into the student and teacher networks, the original image is cropped in two ways global and local. The global crop consists of more than half of the original image and the local crop contains less than half of it. The global crop and local crop are resized to  $224^2$  and  $96^2$  respectively. Then, they are divided into patches that are independently augmented based on a random selection of photometric augmentations. The resulting global crops are fed to the teacher and the global along local crops are fed to the student network. The networks extract feature representations and through the backpropagation, the student and teacher networks are being trained simultaneously.

### 3.3 Patch-Level Augmentation

In traditional approaches, augmentation is applied uniformly across the entire image, leading to a homogenized perspective where local variations are often masked by global transformations. Our method diverges from this norm by treating each patch as an independent entity, subject to its unique augmentation process. This allows for the creation of a more complex and varied training dataset, where each patch can exhibit variations that are not necessarily correlated with the global image context. This independent patch-level

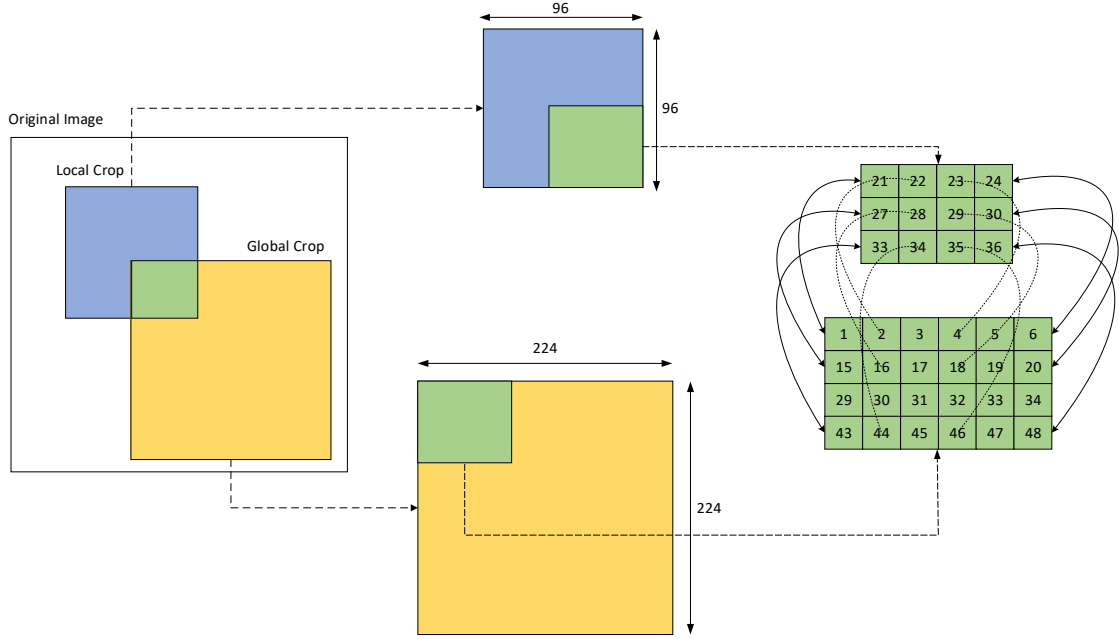


Figure 2 The original image is augmented in two ways local and global. The local crop (blue rectangle) contains less than 50% of the original image while the global crop (yellow rectangle) contains more than 50% of it. Then, they are resized to  $96^2$  and  $224^2$  respectively. To find the corresponding patches across the local and global crops, the intersection area (green rectangle) is determined. The intersection area includes separate patches for the local and global crops. Assuming the patch size is 16, the intersection area contains some patches ranging from 21 to 36 from the local crop and some patches from 1 to 48 from the global crop. To determine the corresponding patches, we select rows/columns at specific intervals. This interval is calculated by dividing the total number of rows/columns in the global crop by the number of rows/columns in the local crop minus one (Eq. 2, Eq. 3). To select the desired rows or columns, we multiply integer numbers (0, 1, 2, etc.) by the interval and round down to the nearest whole number (Eq. 4 and Eq. 5). As a result, the 1<sup>st</sup>, 2<sup>nd</sup>, and 4<sup>th</sup> rows, and the 1<sup>st</sup>, 2<sup>nd</sup>, 4<sup>th</sup>, and 6<sup>th</sup> columns are selected.

augmentation technique is particularly advantageous in scenarios involving complex scenes with diverse elements. By exposing the model to a broader spectrum of variations at the patch level, we equip it with a more refined understanding of local features, enhancing its ability to distinguish subtle differences in texture, shape, and color.

In the patch-level augmentation, the views are divided into patches. Each patch is treated as a standalone unit, undergoing its unique augmentation process. This stage is characterized by the exclusive use of photometric augmentations, which alter the appearance of the patches without affecting their spatial position. Photometric augmentations encompass a variety of operators, including color jittering, solarization, blurring, and Gaussian noise. Each patch independently undergoes a random selection from these operators, ensuring that no two patches necessarily undergo the same combination of augmentations. Patch-level augmentation increases the diversity of the local regions e.g., object parts within images. By learning to minimize the distance between corresponding patches across various augmentations, the model develops an invariance to different augmentation combinations. Hence, it can be generalized well.

### 3.4 Patch-Matching Algorithm

Among the two phases of spatial and photometric augmentations, only the spatial augmentations affect the positions of pixels. As a result, the patch-matching algorithm described in this section only accounts for the operators inside the spatial augmentations which are crop, resize, and horizontal flip. Figure 2 illustrates our patch-matching algorithm applied to an original image subjected to random crop and resize. Figure 3 shows the result of its execution on a real image. Identifying corresponding patches between the global and local crops hinges on finding their overlapping area. If there is no overlap, the only matching elements are the CLS tokens. To pinpoint the overlap, we determine which portions of the original image were cropped. By calculating the overlap between the pixel ranges of the local and global crops, we identify the intersection area (depicted as a green rectangle in Figure 2). If  $(x_{min}, y_{min}, x_{max}, y_{max})$  and  $(x'_{min}, y'_{min}, x'_{max}, y'_{max})$  represents the pixel coordinates of global and local crops respectively, the intersection area is calculated by finding the overlapping pixel ranges between them:

$$intersection\ area = [\max(x_{min}, x'_{min}), \max(y_{min}, y'_{min}), \min(x_{max}, x'_{max}), \min(y_{max}, y'_{max})] \quad Eq. 1$$

The intersection area includes separate patches for the local and global crops. Even if this area does not cover an entire patch at the rectangle's edges, we consider a patch part of the intersection if it includes more than half of its width and height. In the example Figure 2, assuming the patch size 16, the intersection area contains patches ranging between 21 to 36 from the local and between 1 to 48 from the global crops. These patches are distributed across 3 rows and 4 columns in the local and 4 rows and 6 columns in the global crops.

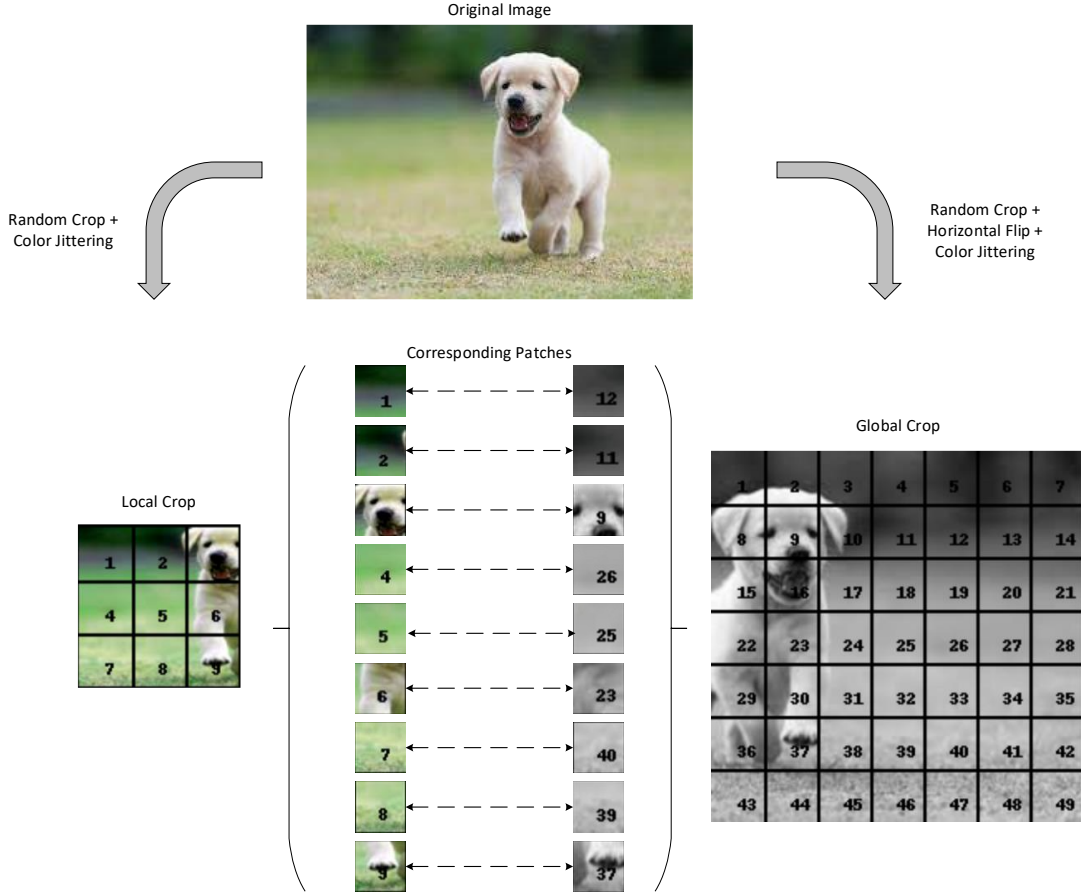


Figure 3 The result of performing the proposed patch-matching algorithm on a real image. The local crop results by performing random crop and color jittering on the original image, while the global includes these operators as well as horizontal flip. In this example, the global crop contains the whole local crop. As a result, all patches inside the local crop are matched with their corresponding patches in the global variant. For instance, patch #3 of the local is matched with patch #9 of the global where both contain the dog's face. As another example, patch #9 of the local is matched with patch #37 of the global, where both contain dog's hands.

In the patch-matching algorithm, the aim is to match the patches of one view with the other view uniformly. This is done by selecting some of the patches within the view with more rows/columns to be matched with all patches within the view with fewer rows/columns while ensuring that the first and last rows/columns are matched together. Since the local crop is smaller than the global, it usually contains fewer rows/columns in the intersection area. However, there might be cases where the global crop has fewer rows/columns. To determine the corresponding patches along the rows, we select rows at specific intervals. This interval is calculated by dividing the total number of rows in the global crop by the number of rows in the local crop minus one (Eq. 2). The same approach is used for columns as well (Eq. 3). However, if the number of rows or columns in the intersection area of the local crop is greater, we calculate the interval by dividing the number of rows or columns in the local crop by the number of rows or columns in the global crop minus one. To select the desired rows or columns, we multiply integer numbers (0, 1, 2, etc.) by the interval and round down to the nearest whole number (Eq. 4 and Eq. 5).

$$\text{row interval} = \frac{\#(\text{global crop rows})}{\#(\text{local crop rows}) - 1} \quad \text{Eq. 2}$$

$$\text{column interval} = \frac{\#(\text{global crop columns})}{\#(\text{local crop columns}) - 1} \quad \text{Eq. 3}$$

$$\text{selected rows} = \lfloor i \times \text{row interval} \rfloor, i = 0, 1, 2, \dots \quad \text{Eq. 4}$$

$$\text{selected columns} = \lfloor i \times \text{column interval} \rfloor, i = 0, 1, 2, \dots \quad \text{Eq. 5}$$

If a horizontal flip is applied to the local or global crops, it merely reverses the sequence of patches in the affected image. For a patch  $P(i, j)$ , the flipped position is calculated as:

$$P'(i, j) = P(i, \#rows - j) \quad \text{Eq. 6}$$

### 3.5 Loss Function Setup

Our framework leverages knowledge distillation, an effective technique for training deep learning models. In this setup, we utilize a dual-network architecture comprising a teacher network and a student network, both of which are trained simultaneously. The teacher network is not pre-trained; instead, it learns concurrently with the student network. To update the teacher network’s parameters efficiently, we employ the Exponential Moving Average (EMA) method. This approach has been explored in various models [8, 21, 30, 49] and is particularly well-suited for our framework, ensuring synchronized and effective learning between the two networks. The update rule is as follows:  $\theta_t \leftarrow \lambda\theta_t + (1 - \lambda)\theta_s$  where  $\theta_t$ ,  $\theta_s$  denote the parameters of the teacher and student networks respectively, and  $\lambda$  follows a cosine schedule. Also, to avoid collapse the centering and sharpening operators have been used. By feeding an image to the network, the probability distribution  $P$  results due to the softmax function as the ultimate layer:  $P_s(x)^i = \frac{\exp(\theta_s(x)^i/\tau_s)}{\sum_{k=1}^K \exp(\theta_s(x)^k/\tau_s)}$  where  $i$  denotes the  $i^{th}$  dimension of the distribution,  $\tau_s$  is the temperature parameter of the student controlling the sharpness of the output distribution. The teacher network shares the same structure with the difference that the centering operator  $C$  is also involved:  $P_t(x)^i = \frac{\exp((\theta_t(x)^i - C)/\tau_t)}{\sum_{k=1}^K \exp((\theta_t(x)^k - C)/\tau_t)}$  where  $C$  is the average of samples inside the batch.

If  $x_i$  is the  $i^{th}$  image in the batch, by performing augmentations on that,  $x_i^{g(j)}, x_i^{l(j)}$  obtain which are the  $j^{th}$  global and local crops of  $x_i$  respectively. In our implementation, 2 global and 8 local crops are extracted. These 2 global crops are passed through both the teacher and student networks. The results are  $g_i^j = P_t(x_i^{g(j)}), j = 1, 2$  and  $gs_i^j = P_s(x_i^{g(j)}), j = 1, 2$  respectively. The 8 local crops are only fed to the student network where the results are  $ls_i^j = P_s(x_i^{l(j)}), j = 1, 2, \dots, 8$ . Hence the outputs of the student network are  $l_i^j = [gs_i^1, gs_i^2, ls_i^1, ls_i^2, \dots, ls_i^8]$ ; where the first two elements are the results of feeding global crops and the eight remaining are from feeding local crops. Then, the loss between the outputs of teacher and student is calculated using the cross-entropy loss  $H(a, b) = -a \log(b)$ .

In the DINO loss function (Eq. 7), the cross entropy between the CLS representations (token 0) of the outputs of teacher and student are calculated. Two cases are excluded from the loss calculations ( $2 \times 10 - 2 = 18$ ). Those are when  $i = j = 1$  and  $i = j = 2$ . The reason is that in both cases, the student and teacher have been operated on the same view. The mentioned operation is repeated for every image in the batch. The final loss is the average of the calculated terms.

$$\text{DINO Loss} = \frac{\sum_{b=1}^{\text{batch-size}} \sum_{i=1}^2 \sum_{j=1, j \neq i}^{10} H(g_b^i[0], l_b^j[0])}{\text{batch-size} \times 18} \quad \text{Eq. 7}$$

In the patch-wise mean loss (Eq. 8), the same operations are done with the difference that for every global and local crop, the correspondent patches have been calculated and stored in  $g_b^i$  and  $l_b^j$ . Hence the cross-entropy between all the matched patches (including CLS plus other tokens) are calculated. The final loss is the average between those terms.

$$\text{Patch-Wise Mean Loss} = \frac{\sum_{b=1}^{\text{batch-size}} \sum_{i=1}^2 \sum_{j=1, j \neq i}^{10} (\sum_{p=0}^{\#(\text{matched-patches})-1} H(g_b^i[p], l_b^j[p]) / \#(\text{matched-patches}))}{\text{batch-size} \times 18} \quad \text{Eq. 8}$$

In the patch-wise sum loss (Eq. 9), the only difference w.r.t. the patch-wise mean loss (Eq. 8) is that the final loss comes from the summation of the cross-entropy terms but is not divided by the number of matched patches.

$$\text{Patch-Wise Sum Loss} = \frac{\sum_{b=1}^{\text{batch-size}} \sum_{i=1}^2 \sum_{j=1, j \neq i}^{10} \sum_{p=0}^{\#(\text{matched-patches})-1} H(g_b^i[p], l_b^j[p])}{\text{batch-size} \times 18} \quad \text{Eq. 9}$$

In both patch-wise mean loss (Eq. 8) and patch-wise sum loss (Eq. 9), each cross-entropy term contributes to the final loss equally. However, in patch-wise  $\lambda$  loss (Eq. 10), we differentiate between the CLS tokens and other tokens’ weights. This is done by giving weight  $\lambda$  to the CLS tokens and weight  $1 - \lambda$  to others.

$$\text{Patch-Wise Lambda } (\lambda) \text{ Loss} = \frac{\sum_{b=1}^{\text{batch-size}} \sum_{i=1}^2 \sum_{j=1, j \neq i}^{10} (\lambda \times H(g_b^i[0], l_b^j[0]) + (1 - \lambda) \times \left( \frac{\sum_{p=1}^{\#(\text{matched-patches})-1} H(g_b^i[p], l_b^j[p])}{\#(\text{matched-patches})-1} \right))}{\text{batch-size} \times 18} \quad \text{Eq. 10}$$

A pseudo-code implementation is proposed in Algorithm 1 for better comprehension of the algorithm.

```

1  gt.params = gs.params # gs, gt: student and teacher networks
2  for b in loader: # load a minibatch b with n samples
3  [b1, cropped_coords1, flipped1] = augment(b) # b1 random view, cropped_coords1 cropped area coordinates in b1, flipped1 is 1 if flipped else 0
4  [b2, cropped_coords2, flipped2] = augment(b) # b2 random view, cropped_coords2 cropped area coordinates in b2, flipped2 is 1 if flipped else 0
5  # find correspondent patches:
6  correspondences = patch_matching([b1, cropped_coords1, flipped1], [b2, cropped_coords2, flipped2])
7  t = gt(b1) # teacher output n x m x K => n samples in the batch - m number of patches+1 - K dimensions
8  s = gs(b2) # student output n x m x K => n samples in the batch - m number of patches+1 - K dimensions
9  # calculate loss:
10 loss = H(t, s, correspondences)
11 loss.backward() # back-propagate
12
13 def H(t, s, correspondences):
14 t = t.detach() # stop gradient
15 # Select Correspondent Patches:
16 t_selected_patches = t[:, correspondences.selected_crop1_patches, :]
17 s_selected_patches = s[:, correspondences.selected_crop2_patches, :]
18 # Softmax student and teacher selected patches outputs:
19 t_softmax = softmax((t_selected_patches - C) / tpt, dim=-1) # centering + sharpening, C: center (K), tpt: teacher temperature
20 s_softmax = log_softmax(s_selected_patches / tps, dim=-1) # tps: student temperature
21 # Calculate Loss:
22 cross_entropy_loss = - t_softmax * s_softmax
23 loss_tensor = torch.sum(cross_entropy_loss, dim=-1) # Summation over dimensions
24 final_loss = loss_formula(loss_tensor) # loss_formula: Mean (Eq. 8) or Sum (Eq. 9) or Lambda ( $\lambda$ ) (Eq. 10)
25 return final_loss

```

## 4. Results

### 4.1 Experimental Setup

#### 4.1.1 Datasets

The datasets used in this work are in common with related works in the literature. We have used three datasets Cifar10, ImageNet-100, and ImageNet-1K to pretrain our network. Cifar10 is a small-scale dataset that has 10 classes with images in 32×32 resolutions. It has 60,000 images of which 50,000 are for training and 10,000 for validation. ImageNet-1K is an image dataset that aligns with the WordNet hierarchy. Each synset represents a meaningful concept and is associated with one or more words or word phrases. ImageNet's primary goal is to offer an average of 1,000 curated images for each synset, all of which undergo quality control and human annotation. It encompasses 1000 object classes and comprises 1,281,167 training images, 50,000 validation images, and 100,000 test images. ImageNet-100 is a subset of the ImageNet-1K dataset that has 100 classes randomly selected. The dataset is well-balanced such that each class contains 1,300 training images and 50 validation images.

#### 4.1.2 Implementation Details

In order to find the patch correspondences across the global and local crops, it is necessary first to find the intersection area between the global and local crops. For that, it is needed to return the cropped area (start and end pixels for both the width and height), randomly chosen from the original image when performing random crop operation. These parameters are not returned by default in deep learning frameworks *TensorFlow* and *PyTorch*. As a result, we overwrote the original implementation of the method in *PyTorch*. By doing so, we could find the intersection area between each crop extracted from the original image.

In our proposed method, the patch-matching algorithm identifies corresponding patches for images within a mini-batch, followed by computing cross-entropy loss for each pair of matched patches. This step is typically time-intensive due to its incompatibility with vectorization techniques, unlike the DINO framework, which matches only CLS tokens without seeking matched patches. To address the issue, we implemented a simplification in our algorithm: all images in a batch undergo identical spatial augmentations. This is achieved by enforcing the same random seed for spatial augmentation operators: resize, crop, and horizontal flip across all samples in a batch. For instance, if the second global view of the first image in a batch is cropped at certain points, the same applies to the second global view of all other images in the batch. This uniformity means the patch-matching algorithm needs to be applied only once per batch, with the results applicable to all images. This strategy allows for vectorized loss calculations, leading to a substantial reduction in code execution time while not compromising the overall network's performance.

In this work, the Adamw optimizer with batch sizes from 10 to 40 is used for different datasets. The learning rate undergoes a linear ramp-up phase in the initial 10 epochs until it reaches its base value. It decays based on a cosine schedule. Similarly, the weight decay follows a cosine schedule, transitioning from 0.04 to 0.4. The temperature parameter ( $\tau_s$ ) is set at 0.1, and a linear warm-up scheme is applied to the parameter  $\tau_t$ , transitioning from 0.04 to 0.07 for the initial 30 epochs.



## 4.2 Evaluation: Linear and KNN image classification

Like other self-supervised representation learning methods, the PW-Self method is pretrained on a dataset without considering its labels. Here, we pretrained PW-Self on three datasets Cifar10, ImageNet-100, and ImageNet-1K separately. In the next stage, the images of that dataset are fed to the pretrained network, and the features are extracted to classify the images. The classification is done in two manners: 1) Linear validation: an MLP layer is placed on top of the extracted features. Then, it will be trained to classify the images. 2) KNN validation: The features are extracted and frozen. The K-Nearest Neighbors (KNN) with K=10 or 20 is performed on them.

### 4.2.1 Pretraining on Cifar10

Table 1 illustrates the results of validating the frozen features that come from pretraining the network for classifying the Cifar10 dataset after training for 200 epochs. As it is clear, PW-Self, with any loss function, outperforms the DINO and other state-of-the-art methods both in linear validation and KNN validation. An interesting point is that our method (when using the patch-wise mean loss function (Eq. 8)) could obtain more increase w.r.t. DINO when doing KNN validation compared to linear validation. To explain it more, by comparing the results of PW-Self with DINO, (rows 3 and 10 in Table 1), the increase obtained in linear validation is +5.86%, while the increase that happened in KNN validation (K=10) is +7.67%. This phenomenon ascertains that in the situation where there is no additional training phase (like KNN validation), the separability of the representations resulting from PW-Self is higher than DINO.

Table 1 The comparison of PW-Self and state-of-the-art methods when pretrained on Cifar10 for 200 epochs. PW-Self is trained with ViT-Base as the backbone. The experiments are done with various configurations for loss function (patch-wise mean, patch-wise sum, and patch-wise  $\lambda$ ), and patch size 16. Linear validation and KNN validation columns demonstrate the Cifar10 image classification accuracies. In all experiments, the PW-Self outperforms existing approaches.

Pretraining Dataset	Method (backbone/patch-size, loss func.)	Linear Validation	KNN Validation	
			(K=10)	(K=20)
Cifar10	SCLR [9]	86.54	82.81	82.11
	MoCov2 [29]	87.61	83.52	83.74
	DINO (ViT-Base/16, Eq. 7) [21]	87.79	84.44	84.91
	BarlowT [18]	88.74	86.14	85.26
	OBoW [11]	88.81	87.64	86.17
	SwAV [14]	90.13	90.41	88.84
	BYOL [23]	90.41	89.32	90.87
	EsViT (ViT-Base/16) [26]	90.56	90.15	88.27
	ARB [45]	92.19	91.75	91.46
	PW-Self (ViT-Base/16, Mean (Eq. 8))	93.65	<b>92.11</b>	<b>92.07</b>
	PW-Self (ViT-Base/16, Sum (Eq. 9))	92.71	91.21	90.13
PW-Self (ViT-Base/16, $\lambda = 0.2$ (Eq. 10))	<b>93.92</b>	91.85	91.47	

### 4.2.2 Pretraining on ImageNet-100

Table 2 presents the results of the comparison of our method and other state-of-the-art approaches when pretrained on ImageNet-100 after training for 200 epochs. The proposed PW-Self method with the patch-wise mean loss function (Eq. 8) and patch size 16 could outperform other state-of-the-art methods both in linear and KNN validations.

Table 2 The results comparison of PW-Self and state-of-the-art methods when pretrained on ImageNet-100 for 200 epochs. PW-Self is trained with ViT-Base as the backbone, patch-wise mean loss function, and patch size 16. Linear validation and KNN validation columns demonstrate the ImageNet-100 image classification accuracies. PW-Self outperforms existing approaches.

Pretraining Dataset	Method (backbone/patch-size, loss func.)	Linear Validation	KNN Validation	
			(K=10)	(K=20)
ImageNet-100	SCLR [9]	71.72	55.64	55.92
	MoCov2 [29]	74.12	57.65	57.41
	OBoW [11]	75.29	58.43	58.74
	BarlowT [18]	76.91	58.48	58.32
	BYOL [23]	77.52	59.58	59.19
	SwAV [14]	77.68	61.51	61.74
	DINO (ViT-Base/16, Eq. 7) [21]	78.22	68.58	68.84
	ARB [45]	79.48	73.51	73.87
	EsViT (ViT-Base/16) [26]	80.44	71.74	70.24
	MSBReg [42]	81.56	74.51	75.12
	PW-Self (ViT-Base/16, Mean (Eq. 8))	<b>83.46</b>	<b>76.37</b>	<b>76.23</b>

More experiments with various backbone architectures ViT-Tiny, ViT-Small, and ViT-Base are reported in Table 3 to provide more visibility. One interesting point in Table 3 is that the linear validation improvements made by PW-Self in comparison with DINO have been increased by enlarging the number of training parameters. To explain it more, when ViT-Tiny, ViT-Small, and ViT-Base are used as the backbone, the linear validation improvements of PW-Self w.r.t the DINO are +3.75%, +3.78, and +5.24% each in order. This confirms that the PW-Self, due to the injected inductive biases through the learning process, has more capacity to learn the relations in comparison with the DINO.

Table 3 The results comparisons of PW-Self and DINO when pretrained on ImageNet-100 for 200 epochs. Both methods are trained with ViT-Tiny, ViT-Small, and ViT-Base as the backbone. Patch-Wise Mean loss is used as the loss function for PW-Self. Linear validation and KNN validation columns demonstrate the ImageNet-100 image classification accuracies. In all experiments, PW-Self outperforms DINO.

Pretraining Dataset	Method	Backbone	Patch size	Loss Function	Linear Validation	KNN Validation	
						(K=10)	(K=20)
ImageNet-100	DINO [21]	ViT-Tiny	16	Eq. 7	58.08	51.84	52.74
	PW-Self	ViT-Tiny	16	Mean (Eq. 8)	<b>61.83</b>	<b>59.23</b>	<b>59.07</b>
	DINO [21]	ViT-Small	16	Eq. 7	70.92	64.64	64.74
	PW-Self	ViT-Small	16	Mean (Eq. 8)	<b>74.70</b>	<b>68.45</b>	<b>68.28</b>
	DINO [21]	ViT-Base	16	Eq. 7	78.22	68.58	68.84
	PW-Self	ViT-Base	16	Mean (Eq. 8)	<b>83.46</b>	<b>76.37</b>	<b>76.23</b>

### 4.2.3 Pretraining on ImageNet-1K

We pretrained the proposed PW-Self method with ViT-Base, patch size 16, and the patch-wise mean loss function (Eq. 8) on ImageNet-1K for 50 epochs. The linear and KNN validation results are reported in Table 4. As can be seen, PW-Self outperforms other existing methods successfully.

Table 4 The results comparison of PW-Self and state-of-the-art methods when pretrained on ImageNet-1K for 50 epochs. PW-Self is trained with ViT-Base as the backbone, patch-wise mean loss function, and patch size 16. Linear validation and KNN validation columns demonstrate the ImageNet-1K image classification accuracies. PW-Self outperforms existing approaches.

Pretraining Dataset	Method (backbone/patch-size, loss func.)	Linear Validation	KNN Validation	
			(K=10)	(K=20)
ImageNet-1K	SCLR [9]	60.06	52.81	51.16
	BarlowT [18]	61.02	58.71	56.59
	ARB [45]	62.05	63.46	62.51
	MoCov2 [29]	64.53	53.14	52.78
	OBoW [11]	68.76	58.49	57.13
	BYOL [23]	69.87	60.51	60.13
	SwAV [14]	70.84	62.49	61.19
	DINO (ViT-Base/16, Eq. 7) [21]	71.46	64.55	64.34
	EsViT (ViT-Base/16) [26]	73.21	67.49	67.31
	PW-Self (ViT-Base/16, Mean (Eq. 8))	<b>73.51</b>	<b>68.71</b>	<b>68.42</b>

## 4.3 Evaluation: Downstream Tasks

The resulting features can be applied in other image applications as well. In this work, two downstream tasks copy detection and image retrieval are selected to test the generalizability of the representations coming out from the pretrained networks.

### 4.3.1 Copy Detection

This task is to recognize the distortions of types of insertions, blurring, printing, etc. To evaluate the performance of the methods, the mean Average Precision (mAP) is reported on the “strong” subset of the Copydays dataset. Two distinct image sets of 10k and 20k are required to run the task. The 10k set is for distractor images, and the 20k set is for learning the parameters of the whitening operator. When evaluating the networks pretrained on Cifar10 and ImageNet-100, both image sets are randomly sampled from the ImageNet dataset excluding the images contained in the ImageNet-100. Although, when evaluating the network pretrained on ImageNet-1K, the whole ImageNet-1K was used to train those parameters. Table 5 compares the results of the PW-Self with DINO when pretrained on Cifar10, ImageNet-100, and ImageNet-1K respectively. The PW-Self model surpasses DINO when not using patch-level augmentation. A more detailed discussion about the reasons is available in 5.4.

### 4.3.2 Image Retrieval

The revisited Oxford and Paris datasets were used for the image retrieval task. They both contain 3 splits Easy (E), Medium (M), and Hard (H). We report the mean Average Precision (mAP) on Medium and Hard splits, following DINO’s tradition [21]. After pretraining with either DINO or PW-Self, the images of the mentioned datasets were fed to the network. Then, the features are extracted and frozen. Finally, the KNN classifier is applied to retrieve the most relevant images. The mAPs for two datasets are reported in Table 5 when pretraining is done on Cifar10, ImageNet-100, and ImageNet-1K respectively. As can be seen, using the PW-Self method with patch-wise mean loss function (Eq. 8) outperforms DINO in both Medium and Hard splits in both datasets Oxford and Paris.

Table 5 The comparison of downstream tasks results between PW-Self and DINO, when pretrained on Cifar10, ImageNet-100, and ImageNet-1K. The downstream tasks are copy detection and image retrieval. The mAP is reported on the “strong” subset of the copydays (copy detection), and Oxford and Paris (image retrieval) datasets.

Pretraining Dataset	Method	Backbone	Patch size	Patch-level Aug.	Loss Function	Copy Detection	Image Retrieval	
							Oxford	Paris
Cifar10	DINO [21]	ViT-Base	16	-	Eq. 7	0.60	M: 7.52, H: 1.59	M: 19.44, H: 5.23
	PW-Self	ViT-Base	16	✓ ✗	Mean (Eq. 8)	0.54 0.64	M: 8.83, H: 1.73 M: 8.64, H: 1.65	M: 21.51, H: 5.64 M: 21.34, H: 5.28
ImageNet-100	DINO [21]	ViT-Base	16	-	Eq. 7	0.73	M: 13.64, H: 2.50	M: 23.89, H: 7.11
	PW-Self	ViT-Base	16	✓ ✗	Mean (Eq. 8)	0.69 0.76	M: 14.87, H: 3.11 M: 14.12, H: 2.56	M: 25.41, H: 7.50 M: 24.60, H: 7.21
ImageNet-1K	DINO [21]	ViT-Base	16	-	Eq. 7	0.79	M: 25.85, H: 9.13	M: 54.88, H: 27.84
	PW-Self	ViT-Base	16	✓ ✗	Mean (Eq. 8)	0.75 0.81	M: 28.86, H: 9.19 M: 28.66, H: 9.17	M: 58.26, H: 29.73 M: 58.11, H: 29.71

## 5. Discussions

In this section, we discuss the computational complexity of our method and compare it with the most similar approaches in the literature. In addition, the effect of the patch size, backbone architectures, proposed loss functions, and lambda value parameters in the proposed PW-Self method are explored.

### 5.1 Computational Complexity Analysis

Our methodology extends beyond the standard DINO framework by incorporating three additional modules: patch-level augmentation, patch-matching, and enhanced loss function calculation. The patch-level augmentation module exhibits a computational complexity of  $O(T)$ , where  $T$  represents the total number of patches in views. Our patch-matching algorithm, streamlined for efficiency, operates at a constant time complexity  $O(1)$ , owing to its reliance solely on the number of rows and columns in the respective views for effective matching. Moreover, the aggregation of local losses into the overall loss is characterized by a complexity of  $O(Td)$ , with  $d$  denoting the dimensionality of the representations. Consequently, the overall complexity of our proposed method is evaluated at  $O(Td)$ .

In comparison to similar methods such as EsViT [26] and SelfPatch [25], our approach demonstrates greater efficiency. A comparative analysis of computational complexities, as presented in Table 6, reveals that EsViT’s approach, which involves identifying the most similar patch to each anchor patch based on maximal cosine similarity, results in a complexity of  $O(T^2 d)$ . Meanwhile, SelfPatch locates positive pairs by exploring the 8 neighboring patches of the query, leading to a complexity of  $O(8Td)$ . Additionally, it employs a smaller transformer in its aggregation module to derive final representations that lead to a complexity of  $O(T^2 d)$ .

Table 6 The comparison of computational time complexities between EsViT, and SelfPatch which are the most similar methods to the proposed PW-Self method.

Method	Computational Complexity
EsViT [26]	$O(T^2 d)$
SelfPatch [25]	$O(T^2 d)$
PW-Self	$O(Td)$

### 5.2 Effect of Backbone Architecture

The first three rows in Table 9 present the results of PW-Self when pretrained on ImageNet-100 with various backbone architectures while fixing other parameters as constant. The backbone architectures ViT-Tiny, ViT-Small, and ViT-Base are utilized which have 5.8, 22.2, and 86 million parameters respectively. By increasing the training parameters, the opportunity is given to the model to better fit the real representation manifold. Hence, better classification accuracies have been achieved when backbones with more training parameters are used. However, it is important to consider that sometimes more training parameters result in overfitting. This happens when the model has used its capacity and there is no more space to learn. In our case, since a significant increase has occurred when going from ViT-Small to ViT-Base (+8.36%), it can be deduced that there has been space to learn and overfitting is an unlikely situation.

### 5.3 Effect of Patch Size

The impact of the patch size parameter is evident in Table 7 (rows 2 and 5) and Table 9 (rows 3 and 5). In Table 7, when pretraining on Cifar10, a reduction in the patch size from 32 to 16, while maintaining other parameters constant, resulted in a notable increase of +2.37% in linear validation accuracy and +5.34% in KNN validation accuracy. However, in Table 9, pretraining on ImageNet-100 and reducing the patch size from 16 to 8, led to a decrease of -4.27% in linear validation accuracy and -5.36% in KNN validation accuracy. This decline can be attributed to potential overfitting, wherein an excessive reduction in patch size generates an abundance of patch correspondences, each serving as a constraint during model training. The presence of numerous constraints may induce overfitting, thereby compromising model performance. Consequently, a reduction in patch size improves model performance up to a certain threshold; beyond this point, however, further reduction may induce overfitting.

### 5.4 Effect of Patch-level Augmentation

In Table 7 (rows 4 and 5), and Table 9 (rows 3 and 4) the beneficial impact of patch-level augmentation on image classification is illustrated. It shows about a 1% increase in linear and KNN validation accuracies for Cifar10 and ImageNet-100. Conversely, Table 8 (rows 1 and 2) reveals varying effects on downstream tasks. While image retrieval benefits from patch-level augmentation, copy detection experiences a significant decline. This decline is likely due to the conflicting goals of the two approaches. Copy detection focuses on identifying image manipulations, such as altered or distorted sections. Patch-level augmentation, however, is designed to make the model less sensitive to changes in patches, particularly those caused by photometric alterations like color shifts or noise addition. This desensitization means the model may overlook the distortions that copy detection seeks to identify. Thus, patch-level augmentation generally serves as a valuable inductive bias in representation learning, except in scenarios like copy detection where such distortion detection is crucial.

### 5.5 Effect of the Loss Function

Table 7 and Table 8 provide reports to compare the results of integrating the proposed loss functions when pretrained on Cifar10. A general point is that there is not much difference between employing different loss functions. Utilizing each of them can result in prominent results either in linear and KNN classification or downstream tasks. From a practical point of view, the property of not being dependent on the loss function seems critical. Changing the loss function in different situations can increase the performance in the desirable metric, while at the same time not downgrade the performance of other metrics significantly. Utilizing the patch-wise mean loss function (Eq. 8) seems to lead to superior results in KNN classification and image retrieval tasks (both datasets Oxford and Paris). In addition, when using the lambda loss function (Eq. 10), some values of  $\lambda$  (e.g.,  $\lambda=0.5$  or  $0.2$  in Table 7) can lead to better linear validation accuracies compared to when using the mean loss function.

### 5.6 Effect of Lambda ( $\lambda$ ) value

An interesting point in Table 7 is that in the proposed PW-Self method, when using the lambda loss function (Eq. 10), the more the lambda value is decreased, the better performances are obtained. For example, when setting  $\lambda = 0.8$ , the effect of the CLS token in the overall loss value is 80% and the effect of other tokens is 20%. In this case, the linear validation is 76.52%. However, when setting  $\lambda = 0.2$ , the effect of the CLS token is only 20%, and the effect of other tokens is 80%. In this scenario, the linear validation has become 79.65%. This highlights the importance of considering patch representations concerning the CLS token. It verifies the main idea of this paper, which is learning from not only the whole image but also smaller patches inside the image. This point is valid when comparing the results of downstream tasks in Table 8 as well. Thus, by decreasing the lambda value (until 0.2 for image retrieval and 0.5 for copy detection), the mAP values have been increased.

Table 7 The results comparison of PW-Self with different configurations when pretrained on Cifar10. PW-Self is trained with ViT-Tiny as the backbone. The experiments are done with various configurations for loss function (patch-wise mean, sum, and  $\lambda$  with multiple values for  $\lambda$ ), and patch sizes 32 and 16. Linear validation and KNN validation columns demonstrate the Cifar10 image classification accuracies.

Pretraining Dataset	Method	Backbone	Patch size	Patch-level Aug.	Loss Function	Linear Validation	KNN Validation	
							(K=10)	(K=20)
Cifar10	DINO [21]	ViT-Tiny	32	✗	Eq. 7	71.05	72.19	72.67
	PW-Self	ViT-Tiny	32	✗	Mean (Eq. 8)	75.73	77.17	77.24
	DINO [21]	ViT-Tiny	16	✗	Eq. 7	75.29	76.38	76.24
	PW-Self	ViT-Tiny	16	✓	Mean (Eq. 8)	79.23	83.68	83.56
				✗	Mean (Eq. 8)	78.10	82.51	82.41
				✗	Sum (Eq. 9)	78.58	78.86	78.52
				✗	$\lambda = 0.9$ (Eq. 10)	75.87	76.82	76.64
				✗	$\lambda = 0.8$ (Eq. 10)	76.52	76.65	76.94
				✗	$\lambda = 0.5$ (Eq. 10)	79.28	79.10	79.12
				✗	$\lambda = 0.2$ (Eq. 10)	79.65	79.48	79.42
				✗	$\lambda = 0.1$ (Eq. 10)	79.06	79.36	79.04

Table 8 The downstream tasks result comparison of PW-Self with different configurations when pretrained on Cifar10. PW-Self is trained with ViT-Tiny as the backbone. The experiments are done with various configurations for loss function (patch-wise mean, patch-wise sum, and patch-wise  $\lambda$  with multiple values for  $\lambda$ ), and patch size 16. The mAP is reported for copy detection and image retrieval downstream tasks.

Pretrain Dataset	Method	Backbone	Patch size	Patch-level Aug.	Loss Function	Copy Detection	Image Retrieval	
							Oxford	Paris
Cifar10	PW-Self	ViT-Tiny	16	✓	Mean (Eq. 8)	0.50	M: 8.41, H: 1.72	M: 22.04, H: 5.13
				✗	Mean (Eq. 8)	0.59	M: 8.34, H: 1.63	M: 21.18, H: 5.11
				✗	Sum (Eq. 9)	0.53	M: 7.37, H: 1.47	M: 19.28, H: 4.26
				✗	$\lambda = 0.9$ (Eq. 10)	0.58	M: 6.35, H: 1.61	M: 17.71, H: 4.57
				✗	$\lambda = 0.8$ (Eq. 10)	0.59	M: 6.58, H: 1.52	M: 17.85, H: 4.57
				✗	$\lambda = 0.5$ (Eq. 10)	0.59	M: 6.72, H: 1.44	M: 17.51, H: 4.41
				✗	$\lambda = 0.2$ (Eq. 10)	0.58	M: 7.12, H: 1.63	M: 19.37, H: 4.68
				✗	$\lambda = 0.1$ (Eq. 10)	0.57	M: 6.90, H: 1.47	M: 20.15, H: 4.84

Table 9 The results comparison of PW-Self with different configurations when pretrained on ImageNet-100. PW-Self is trained with ViT-Tiny, ViT-Small, and ViT-Base as the backbone. The experiments are done with patch-wise mean loss function, and patch sizes 16 and 8. Linear validation and KNN validation columns demonstrate the ImageNet-100 image classification accuracies.

Pretraining Dataset	Method	Backbone	Patch size	Patch-level Aug.	Loss Function	Linear Validation	KNN Validation	
							(K=10)	(K=20)
ImageNet-100	PW-Self	ViT-Tiny	16	✗	Mean (Eq. 8)	61.52	58.66	58.10
		ViT-Small	16	✗		74.44	67.92	68.16
		ViT-Base	16	✗		82.80	75.24	75.43
		ViT-Base	16	✓		83.46	76.37	76.23
		ViT-Base	8	✗		78.53	69.88	68.78

## 6. Conclusion

In this paper, we presented PW-Self, a patch-wise representation learning algorithm, that explored the benefits of considering patches within the self-supervised representation learning frameworks. In addition to pulling the representations of the whole augmented views, our key idea was to minimize the representation distance between the correspondent local regions, e.g., patches inside the views. This idea served as an inductive bias that could provide the model with useful insights into the details within the images. To generate more diversity in the training images, the augmented crops were passed through a patch-level augmentation module, wherein individual patches are augmented independently, ensuring distinct and varied transformations separate from those applied to other patches. The alignment of corresponding patches among augmented views was achieved through the application of a simple, yet efficient, patch-matching algorithm. Patch-matching algorithm, due to its efficient design, lowers the computational time complexity compared to similar models. As a result, the model not only gains a profound understanding of the details within images but also operates more quickly compared to traditional patch-wise representation learning methods. Our exhaustive experimental assessments across varied datasets validate the effectiveness of our proposed approach. The patch-wise representation learning algorithm showcases its potential by elevating the state-of-the-art in self-supervised representation learning. This is evidenced by improvements in image classification accuracy: an increase of 1.73% on Cifar10, 1.9% on ImageNet-100, and 0.3% on ImageNet-1K. Furthermore, the method demonstrated promising results in downstream tasks such as copy detection and image retrieval.

## 7. Declarations

### 7.1 Conflict of interests

The authors declare that they have no conflict of interest.

### 7.2 Funding

This research did not receive any specific grant from funding agencies in the public, commercial, or not-for-profit sectors.

### 7.3 Data Availability Statement

The data that support the findings of this study are [ImageNet-1K](#) [50], [ImageNet-100](#) [50], and [Cifar10](#) [51] which are openly available.

### 7.4 Declaration of Generative AI and AI-assisted technologies in the writing process

During the preparation of this work, the authors used ChatGPT to improve the quality of the manuscript writing. After using this tool, the authors reviewed and edited the content as needed. They take full responsibility for the content of the publication.

## REFERENCES

1. Wu, M., et al. *Conditional negative sampling for contrastive learning of visual representations*. in *International Conference on Learning Representations (ICLR)*. 2021.
2. Robinson, J., C.-Y. Chuang, S. Sra, and S. Jegelka. *Contrastive learning with hard negative samples*. in *International Conference on Learning Representations (ICLR)*. 2021.
3. Kotar, K., et al. *Contrasting contrastive self-supervised representation learning pipelines*. in *Proceedings of the IEEE/CVF International Conference on Computer Vision*. 2021.
4. Dwibedi, D., et al. *With a little help from my friends: Nearest-neighbor contrastive learning of visual representations*. in *Proceedings of the IEEE/CVF International Conference on Computer Vision*. 2021.
5. Xiong, Y., M. Ren, and R. Urtasun. *Loco: Local contrastive representation learning*. in *Advances in neural information processing systems (NeurIPS)*. 2020.
6. Tian, Y., D. Krishnan, and P. Isola. *Contrastive multiview coding*. in *European conference on computer vision (ECCV)*. 2020. Springer.
7. Kalantidis, Y., et al. *Hard negative mixing for contrastive learning*. in *Advances in Neural Information Processing Systems (NeurIPS)*. 2020.
8. He, K., et al. *Momentum Contrast for Unsupervised Visual Representation Learning*. in *IEEE/CVF Conference on Computer Vision and Pattern Recognition (CVPR)*. 2020.
9. Chen, T., S. Kornblith, M. Norouzi, and G. Hinton. *A simple framework for contrastive learning of visual representations*. in *International Conference on Machine Learning (ICML)*. 2020. PMLR.
10. Oord, A.v.d., Y. Li, and O. Vinyals. *Representation learning with contrastive predictive coding*. in *Advances in Neural Information Processing Systems (NeurIPS)*. 2018.
11. Gidaris, S., et al. *Obow: Online bag-of-visual-words generation for self-supervised learning*. in *Proceedings of the IEEE/CVF Conference on Computer Vision and Pattern Recognition (CVPR)*. 2021.
12. Yan, X., et al. *Clusterfit: Improving generalization of visual representations*. in *Proceedings of the IEEE/CVF Conference on Computer Vision and Pattern Recognition (CVPR)*. 2020.
13. Li, J., et al. *Prototypical Contrastive Learning of Unsupervised Representations*. in *International Conference on Learning Representations (ICLR)*. 2020.
14. Caron, M., et al. *Unsupervised learning of visual features by contrasting cluster assignments*. in *Advances in Neural Information Processing Systems (NeurIPS)*. 2020.
15. Caron, M., P. Bojanowski, A. Joulin, and M. Douze. *Deep clustering for unsupervised learning of visual features*. in *Proceedings of the European Conference on Computer Vision (ECCV)*. 2018.
16. Bardes, A., J. Ponce, and Y. LeCun. *Vicreg: Variance-invariance-covariance regularization for self-supervised learning*. in *International Conference on Learning Representations (ICLR)*. 2022.
17. Zhang, S., et al. *Zero-CL: Instance and Feature decorrelation for negative-free symmetric contrastive learning*. in *International Conference on Learning Representations (ICLR)*. 2021.
18. Zbontar, J., et al. *Barlow twins: Self-supervised learning via redundancy reduction*. in *International Conference on Machine Learning (ICML)*. 2021. PMLR.
19. Ermolov, A., A. Siarohin, E. Sangineto, and N. Sebe. *Whitening for self-supervised representation learning*. in *International Conference on Machine Learning (ICML)*. 2021. PMLR.
20. Chen, X. and K. He. *Exploring simple siamese representation learning*. in *Proceedings of the IEEE/CVF Conference on Computer Vision and Pattern Recognition (CVPR)*. 2021.
21. Caron, M., et al. *Emerging Properties in Self-Supervised Vision Transformers*. in *Proceedings of the IEEE International Conference on Computer Vision (ICCV)*. 2021.
22. Azabou, M., et al., *Mine your own view: Self-supervised learning through across-sample prediction*. CoRR, 2021. **abs/2102.10106**.
23. Grill, J.-B., et al. *Bootstrap your own latent: A new approach to self-supervised learning*. in *Advances in Neural Information Processing Systems (NeurIPS)*. 2020.
24. Bachman, P., R.D. Hjelm, and W. Buchwalter. *Learning representations by maximizing mutual information across views*. in *Advances in Neural Information Processing Systems (NeurIPS)*. 2019.
25. Yun, S., H. Lee, J. Kim, and J. Shin. *Patch-Level Representation Learning for Self-Supervised Vision Transformers*. in *Proceedings of the IEEE/CVF Conference on Computer Vision and Pattern Recognition (CVPR)*. 2022.
26. Li, C., et al. *Efficient self-supervised vision transformers for representation learning*. in *Proceedings of the International Conference on Learning Representations (ICLR)*. 2022.
27. Zhang, T., et al. *Leverage your local and global representations: A new self-supervised learning strategy*. in *Proceedings of the IEEE/CVF Conference on Computer Vision and Pattern Recognition*. 2022.
28. Chen, T., et al. *Big self-supervised models are strong semi-supervised learners*. in *Advances in Neural Information Processing Systems (NeurIPS)*. 2020.
29. Chen, X., H. Fan, R. Girshick, and K. He. *Improved baselines with momentum contrastive learning*. CoRR, 2020. **abs/2003.04297**.
30. Chen, X., S. Xie, and K. He. *An empirical study of training self-supervised vision transformers*. in *Proceedings of the IEEE/CVF Conference on Computer Vision and Pattern Recognition (CVPR)*. 2021.

31. Jang, J., et al. *Self-distilled self-supervised representation learning*. in *Proceedings of the IEEE/CVF Winter Conference on Applications of Computer Vision*. 2023.
32. Tian, Y., et al. *What makes for good views for contrastive learning?* in *Advances in Neural Information Processing Systems (NeurIPS)*. 2020.
33. Peng, X., et al. *Crafting better contrastive views for siamese representation learning*. in *Proceedings of the IEEE/CVF Conference on Computer Vision and Pattern Recognition (CVPR)*. 2022.
34. Wang, W., et al. *Instance-wise Hard Negative Example Generation for Contrastive Learning in Unpaired Image-to-Image Translation*. in *Proceedings of the IEEE/CVF Conference on Computer Vision and Pattern Recognition (CVPR)*. 2021.
35. Huynh, T., et al. *Boosting contrastive self-supervised learning with false negative cancellation*. in *Proceedings of the IEEE/CVF winter conference on applications of computer vision*. 2022.
36. Long, X., H. Du, and Y. Li, *Two momentum contrast in triplet for unsupervised visual representation learning*. *Multimedia Tools and Applications*, 2023: p. 1-14.
37. Pöppelbaum, J., G.S. Chadha, and A. Schwung, *Contrastive learning based self-supervised time-series analysis*. *Applied Soft Computing*, 2022. **117**: p. 108397.
38. Feng, W., X. Ma, X. Li, and C. Zhang, *A representation learning framework for stock movement prediction*. *Applied Soft Computing*, 2023: p. 110409.
39. Xie, J., R. Girshick, and A. Farhadi. *Unsupervised deep embedding for clustering analysis*. in *International Conference on Machine Learning (ICML)*. 2016. PMLR.
40. Mo, S., Z. Sun, and C. Li. *Multi-level contrastive learning for self-supervised vision transformers*. in *Proceedings of the IEEE/CVF Winter Conference on Applications of Computer Vision*. 2023.
41. Hsieh, C.-Y., C.-J. Chang, F.-E. Yang, and Y.-C.F. Wang. *Self-Supervised Pyramid Representation Learning for Multi-Label Visual Analysis and Beyond*. in *Proceedings of the IEEE/CVF Winter Conference on Applications of Computer Vision*. 2023.
42. Moon, S., et al. *An Embedding-Dynamic Approach to Self-Supervised Learning*. in *Proceedings of the IEEE/CVF Winter Conference on Applications of Computer Vision*. 2023.
43. Jing, L., P. Vincent, Y. LeCun, and Y. Tian, *Understanding dimensional collapse in contrastive self-supervised learning*. arXiv preprint arXiv:2110.09348, 2021.
44. Chen, F., N. Wang, J. Tang, and F. Zhu, *A feature disentangling approach for person re-identification via self-supervised data augmentation*. *Applied Soft Computing*, 2021. **100**: p. 106939.
45. Zhang, S., et al. *Align Representations with Base: A New Approach to Self-Supervised Learning*. in *Proceedings of the IEEE/CVF Conference on Computer Vision and Pattern Recognition (CVPR)*. 2022.
46. Wang, F., et al., *Self-Supervised Learning by Estimating Twin Class Distributions*. *CoRR*, 2021. **abs/2110.07402**.
47. Liu, H., et al., *Self-supervised learning for fair recommender systems*. *Applied Soft Computing*, 2022. **125**: p. 109126.
48. Amrani, E. and A. Bronstein. *Self-Supervised Classification Network*. in *European Conference on Computer Vision (ECCV)*. 2022.
49. Oquab, M., et al., *Dinov2: Learning robust visual features without supervision*. arXiv preprint arXiv:2304.07193, 2023.
50. Russakovsky, O., et al., *Imagenet large scale visual recognition challenge*. *International journal of computer vision*, 2015. **115**: p. 211-252.
51. Krizhevsky, A. and G. Hinton, *Learning multiple layers of features from tiny images*. 2009.